A. Mahmoud, A. Erba, Kh. E. El-Kelany, M. Rerat, R. Orlando
Low-temperature phase of BaTiO3: Piezoelectric, dielectric, elastic, and photoelastic properties from ab initio simulations
PHYSICAL REVIEW. B, CONDENSED MATTER AND MATERIALS PHYSICS (2014) 89
DOI: 10.1103/PhysRevB.89.045103

Low-temperature Phase of $BaTiO_3$: Piezoelectric, Dielectric, Elastic and Photoelastic Properties from Ab initio Simulations

A. Mahmoud,[1,*] A. Erba,[1] Kh. E. El-Kelany,[2,3] M. Rérat,[2] and R. Orlando[1]

[1] *Dipartimento di Chimica and Centre of Excellence NIS (Nanostructured Interfaces and Surfaces), Università di Torino, via Giuria 5, IT-10125 Torino (Italy)*

[2] *Equipe de Chimie Physique, IPREM UMR 5254, Université de Pau et des Pays de l'Adour, FR-64000 Pau (France)*

[3] *Chemistry Department, Faculty of Science, Minia University, Minia 61519 (Egypt)*

(Dated: December 10, 2013)

A complete theoretical characterization of dielectric, elastic, photoelastic and piezoelectric tensors of the low-temperature rhombohedral phase of $BaTiO_3$ was performed by accurate *ab initio* simulations within periodic boundary conditions, using one-electron Hamiltonians and atom-centered Gaussian-type-function basis sets as in the CRYSTAL program. Because this phase is stable only at very low temperature, experimental characterization is difficult and none of such tensorial properties have been measured. For this reason, we validated our method by comparing structural, electronic and vibrational properties of the other three phases of $BaTiO_3$ (cubic, tetragonal and orthorhombic) with available experimental data. The effect of the adopted one-electron Hamiltonian on the considered tensorial properties, beyond the simple local density approximation and the dependence on the electric field frequency of dielectric and photoelastic constants are explicitly investigated.

I. INTRODUCTION

Barium titanate, $BaTiO_3$, is one of the most studied ferroelectric ceramics. This material is widely used in advanced technological applications as capacitor or component of non-linear optical, piezoelectric and energy/data-storage devices.[1–4] Since the discovery of its ferroelectric character, a lot of attention has been devoted to the peculiar dielectric and piezoelectric properties of $BaTiO_3$.[5]

From a structural point of view, $BaTiO_3$ shows a cubic ABO_3-type perovskite crystal structure at high temperature where A sites host divalent cations (Ba^{2+} in this case) and B sites are occupied by tetravalent cations (Ti^{4+} in this case). With reference to the conventional cubic cell at high temperature, Ba^{2+} ions are placed at corners, O^{2-} ions at the center of faces, thus forming an octahedron, and a Ti^{4+} ion at the body center of the cell.

Upon cooling, three consecutive ferroelectric transitions occur starting from the cubic structure, due to the displacement of Ti ions along different crystallographic directions, the resulting macroscopic polarization of the material being always parallel to this displacement.[6] At 393 K, $BaTiO_3$ undergoes the first transition from a cubic paraelectric to a tetragonal ferroelectric phase, which corresponds to a small structural elongation along a [001] crystallographic direction. Then, an orthorhombic ferroelectric phase occurs between 278 K and 183 K that can be interpreted as a deformation along a face diagonal [011] direction.[7] Finally, below 183 K, $BaTiO_3$ transforms into a low-temperature ferroelectric rhombohedral phase characterized by an elongation along the cell body diagonal [111] direction. Two models have been proposed for phase transitions of $BaTiO_3$: the displacive model[8] is governed by a Γ point soft phonon mode; the order-disorder model[9–11] implies the coexistence of local configurations with lower symmetry with respect to the macroscopic order parameter, that is, the macroscopic polarization in this case.

The structure of the paraelectric cubic phase of $BaTiO_3$ was refined experimentally long time ago.[12,13] Single-crystal X-ray and neutron diffraction structural studies of the tetragonal,[14–16] orthorhombic[17] and rhombohedral[18,19] ferroelectric phases of $BaTiO_3$ have been reported. Among others, the neutron diffraction study of the three ferroelectric phases performed by Kwei *et al.*[6] in 1993 is here taken as a reference as regards their structural properties. Several computational studies of the structures of the different phases of $BaTiO_3$ have also been reported, either with an atom-centered Gaussian-type function (GTF)[20–23] or a plane-wave pseudopotential[24–31] basis set approach. Many of the above-mentioned theoretical studies have also investigated the phonon properties of the cubic phase,[20,21,25,26,28] whereas no experimental spectroscopic measurements are known. Raman scattering experiments have been performed for the tetragonal,[32,33] orthorhombic[34] and rhombohedral[35] phases. As regards theoretical investigations of vibrational frequencies, several studies have addressed this topic for the tetragonal,[20,36–38] orthorhombic[20] and rhombohedral[20,22,31,38,39] phases.

Elastic, piezoelectric and dielectric constants of cubic,[40] tetragonal[41–43] and orthorhombic[44] phases of $BaTiO_3$ have been measured experimentally. In particular, a complete set of dielectric, elastic, piezoelectric, electro-optic and elasto-optic constants has been determined for the ferroelectric tetragonal phase by Zgonik *et al.*[43] The temperature dependence of different elasto-optic tensor components of the cubic phase has been measured also by Cohen *et al.*[45] None of these tensorial properties have been measured experimentally for the low-temperature rhombohedral phase, yet.

A couple of computational studies have been reported

on such tensorial properties of the rhombohedral phase. Wang *et al.*[46] computed elastic, polarization and electrostrictive properties of the four different phases of $BaTiO_3$ by using a local density approximation (LDA), with projector-augmented waves (PAW) and density-functional perturbation theory (DFPT). Elastic, dielectric and piezoelectric properties of the low-temperature ferroelectric rhombohedral phase have been reported by Wu *et al.*[31] who used the same LDA-DFPT approach. In both cases, cell volumes were taken at the experimental values.

In this paper, beside structural, electronic and vibrational properties of the four phases, we focus on accurate *ab initio* simulation of tensorial properties, such as dielectric, elastic, piezoelectric and photoelastic, of the low-temperature rhombohedral phase of $BaTiO_3$. Both electronic and nuclear contributions to these properties are computed and discussed. Recent developments by some of us of fully automated algorithms for the calculation of such tensorial properties in the CRYSTAL program make now such a complete theoretical investigation feasible at relatively low computational cost.[47–50]

The effect of the adopted one-electron Hamiltonian on these tensorial properties is investigated systematically here for the first time beyond the simple LDA approach. In particular, four one-electron Hamiltonians are considered which are representative of four different classes: the reference Hartree-Fock (HF) method, LDA and generalized-gradient approximation (GGA) to the density functional theory (DFT), namely Perdew-Burke-Ernzerhof (PBE),[51] and a global hybrid functional (PBE0) with 25 % of exact HF exchange.[52] All the calculations reported in this manuscript have been performed with a development version of the CRYSTAL program.[53,54] A fairly similar computational approach has been successfully adopted by Evarestov and Bandura for computing structural, thermodynamical and phonon properties of the rhombohedral phase of $BaTiO_3$.[20–22]

The structure of the paper is as follows: in Section II we briefly illustrate the theoretical methods used for the calculation of structural parameters, dielectric, elastic, piezoelectric and photoelastic constants and we report the main computational parameters adopted for these calculations; in Section III A, the major outcomes of structural parameters and phonon frequencies for the four different phases of $BaTiO_3$ are presented; in the following subsections elastic, piezoelectric and photoelastic properties of the low-temperature rhombohedral phase are presented and dicussed. Conclusions are drawn in Section IV.

II. COMPUTATIONAL METHOD AND DETAILS

All the calculations reported in this paper are performed with a development version of the CRYSTAL program for *ab initio* quantum chemistry of solid state.[53,54] An atom-centered Gaussian-type-function (GTF) basis set is adopted whose coefficients for valence electrons have been re-optimized for the cubic phase of $BaTiO_3$, by minimizing the HF energy using the LoptCG script.[55] Oxygen atoms are described by a split-valence 8-411G(2d1f) basis set, Titanium atoms by a 86-411G(3d1f) one while core and valence electrons of Barium atoms are described by a Hay-Wadt small-core pseudopotential[56–58] and 311G(1d1f) functions, respectively.[59]

In CRYSTAL, the truncation of infinite lattice sums is controlled by five thresholds $T_1, \ldots, T_5$; here $T_1 = T_2 = T_3 = 10^{-10}$ a.u., $T_4 = 10^{-12}$ a.u. and $T_5 = 10^{-24}$ a.u. Reciprocal space is sampled according to a sub-lattice with shrinking factor 8, corresponding to 35, 75, 105 and 65 points in the irreducible Brillouin zone for cubic, tetragonal, orthorhombic and rhombohedral phases, respectively. The DFT exchange-correlation contribution is evaluated by numerical integration over the cell volume: radial and angular points of the atomic grid are generated through Gauss-Legendre and Lebedev quadrature schemes, using an accurate predefined pruned grid: the accuracy in the integration procedure can be estimated by evaluating the error associated with the integrated electronic charge density in the unit cell versus the total number of electrons per cell: $3\times10^{-5}|e|$ out of a total number of 56 electrons per cell for the rhombohedral phase, for instance.

A. Dielectric Tensor

The electronic contribution to the static dielectric tensor, at infinite electric field wavelength $\lambda \rightarrow \infty$, is evaluated through a Coupled-Perturbed-HF/Kohn-Sham (CPHF/KS) scheme[60] adapted for periodic systems.[61] From an experimental viewpoint, it corresponds to the dielectric response of the crystal measured for sufficiently high frequencies of the applied electric field to make nuclear contributions negligible, but not high enough for generating electronic excitations. CPHF/KS is a perturbative, self-consistent method that focuses on the description of relaxation of crystalline orbitals under the effect of an external electric field. The perturbed wavefunction is then used to calculate the dielectric properties as energy derivatives. Further details about the method and its implementation in the CRYSTAL program can be found elsewhere[62] as well as some recent example of its application.[48–50,63–65] The electronic dielectric tensor of a 3D crystal is obtained from the polarizability $\boldsymbol{\alpha}$ as:

$$\boldsymbol{\epsilon} = 1 + \frac{4\pi}{V}\boldsymbol{\alpha}\,, \tag{1}$$

where V is the cell volume. With such a scheme, the explicit dependence of the polarizability and dielectric tensors from the electric field wavelength λ can be computed as well.

TABLE I: Fractional atomic coordinates of the symmetry-irreducible atoms of the four different phases of $BaTiO_3$: cubic, tetragonal, orthorhombic and rhombohedral (corresponding space group symbols are also given).

Phase	Cubic	Tetragonal	Orthorhombic	Rhombohedral
Space group	$Pm\overline{3}m$	P4mm	Amm2	R3m
Atomic positions	Ba (0, 0, 0) Ti ($\frac{1}{2}$, $\frac{1}{2}$, $\frac{1}{2}$) O ($\frac{1}{2}$, $\frac{1}{2}$, 0)	Ba (0, 0, 0) Ti ($\frac{1}{2}$, $\frac{1}{2}$, $\frac{1}{2}+\Delta z_{Ti}$) O_1 ($\frac{1}{2}$, $\frac{1}{2}$, Δz_{O1}) O_2 ($\frac{1}{2}$, 0, $\frac{1}{2}+\Delta z_{O2}$)	Ba (0, 0, 0) Ti ($\frac{1}{2}$, 0, $\frac{1}{2}+\Delta z_{Ti}$) O_1 (0, 0, $\frac{1}{2}+\Delta z_{O1}$) O_2($\frac{1}{2}$, $\frac{1}{4}+\Delta y_{O2}$, $\frac{1}{4}+\Delta z_{O2}$)	Ba (0, 0, 0) Ti ($\frac{1}{2}+\Delta x_{Ti}$, $\frac{1}{2}+\Delta x_{Ti}$, $\frac{1}{2}+\Delta x_{Ti}$) O ($\frac{1}{2}+\Delta x_O$, $\frac{1}{2}+\Delta x_O$, Δz_O)

B. Elastic, Piezoelectric and Photoelastic Tensors

The elements of the fourth-rank elastic tensor $\mathbb{C}$ for 3D systems are usually defined as second energy density derivatives with respect to pairs of deformations:[66]

$$C_{vu} = \frac{1}{V} \left. \frac{\partial^2 E}{\partial \eta_v \partial \eta_u} \right|_0 , \tag{2}$$

where $\boldsymbol{\eta}$ is the symmetric second-rank pure strain tensor, V the equilibrium cell volume and Voigt's notation is used according to which $v, u = 1, \ldots 6$ ($1 = xx$, $2 = yy$, $3 = zz$, $4 = yz$, $5 = xz$, $6 = xy$). An automated scheme for the calculation of $\mathbb{C}$ (and of $\mathbb{S} = \mathbb{C}^{-1}$, the compliance tensor) has been implemented in the CRYSTAL program that exploits analytical gradients and computes second derivatives numerically.[47,67]

In the linear regime, *direct* $\mathbf{e}$ and *converse* $\mathbf{d}$ piezoelectric tensors describe the polarization $\mathbf{P}$ induced by strain $\boldsymbol{\eta}$ and the strain induced by an external electric field $\mathbf{E}$, respectively:

$$\textit{direct} \quad \text{effect} \qquad \mathbf{P} = \mathbf{e}\,\boldsymbol{\eta} \qquad \text{at constant field} \tag{3}$$

$$\textit{converse} \quad \text{effect} \qquad \boldsymbol{\eta} = \mathbf{d}^T\mathbf{E} \qquad \text{at constant stress} \tag{4}$$

The *direct* and *converse* piezoelectric tensors are connected to each other: $\mathbf{e} = \mathbf{d}\,\mathbb{C}$ and $\mathbf{d} = \mathbf{e}\,\mathbb{S}$. Our approach consists in directly computing the intensity of polarization induced by strain. In CRYSTAL, the polarization can be computed either via localized Wannier functions or via the Berry phase (BP) approach.[68] The latter scheme is adopted in the automated implementation exploited here.[48]

The elements of the Pockels' elasto-optic fourth-rank tensor $\mathbb{P}$ (*i.e.* elasto-optic constants $\{p_{ijkl}\}$) are defined by the relation:

$$\Delta\epsilon^{-1}_{ij} = \sum_{kl} p_{ijkl}\eta_{kl} \ . \tag{5}$$

In the above expression, $\Delta\boldsymbol{\epsilon}^{-1}$ is the difference between the inverse dielectric tensor of a strained and the unstrained equilibrium configuration; $i, j, k, l = x, y, z$ represent Cartesian directions. If Voigt's notation is used, Pockels' tensor becomes a 6×6 matrix like $\mathbb{C}$ and $\mathbb{S}$. An automated implementation in the CRYSTAL program of the calculation of elasto-optic constants is exploited here.[49]

We recall that elastic, piezoelectric and elasto-optic constants can be decomposed into purely electronic "clamped-ion" and nuclear "internal-strain" contributions; the latter measures the effect of relaxation of the relative positions of atoms induced by the strain and can be computed simply by optimizing atomic positions within the strained cell.[69,70]

III. RESULTS AND DISCUSSION

The main objective of this section is that of reporting and discussing the results of accurate *ab initio* simulations of piezoelectric, elastic, dielectric and photoelastic properties of the low-temperature rhombohedral phase of $BaTiO_3$. Given the predictive character of this study, due to the lack of experimental determinations of these tensorial quantities for the low-temperature ferroelectric phase, the accuracy of our theoretical approach will be discussed with respect to structural, electronic and vibrational properties of the four phases of $BaTiO_3$, for which experimental data have been reported. Section III A is devoted to the illustration of the structural and vibrational description of the four phases.

A. Structural and Vibrational Features of the Four Phases

Before illustrating the accuracy of the present simulations in describing structural features of the four phases, let us recall that, at high temperature, $BaTiO_3$ shows a centro-symmetric cubic structure (space group $Pm\overline{3}m$) that can be described by three symmetry-irreducible atoms in the cell: a Ba^{2+} cation is placed at the origin, an O^{2-} anion at the center of a face and a Ti^{4+} cation at the body center of the crystallographic cubic cell.

TABLE II: Structural and electronic properties of the cubic, tetragonal, orthorhombic and rhombohedral phases of $BaTiO_3$, as computed at PBE0 level and compared with experimental data and a previous theoretical determination at the same PBE0 level (see Ref. 20): lattice parameters a, b, c, volume V, bulk modulus B, bandgap E_g and atomic positions as defined in Table I. For the rhombohedral phase, the lattice angle α is also reported. For each ferroelectric phase, the energy difference ΔE_c with respect to the cubic phase is given.

	Calc.	PBE0	Exp.
Cubic ($Pm\overline{3}m$)		(Ref. 20)	
a (Å)	3.980	3.992	3.996[12]
V (Å^3)	63.03	63.62	63.81[12]
B (GPa)	194	189	162[a]-195[b]
E_g (eV)	4.0	4.0	3.2[71]
Tetragonal (P4mm)			
a (Å)	3.960	3.968	3.997[6]
c (Å)	4.097	4.137	4.031[6]
V (Å^3)	64.24	65.14	64.41[6]
Δz_{Ti}	0.0202	0.0203	0.0203[6]
Δz_{O1}	-0.0391	-0.0431	-0.0258[6]
Δz_{O2}	-0.0202	-0.0226	-0.0123[6]
B (GPa)	117	112	134[c]-141[43]
E_g (eV)	4.2	4.1	3.4[71]
ΔE^c (mHa)	-1.24	-1.51	-
Orthorhombic (Amm2)			
a (Å)	3.951	3.958	3.983[6]
b (Å)	5.696	5.728	5.675[6]
c (Å)	5.729	5.770	5.692[6]
V (Å^3)	128.91	130.81	128.63[6]
Δz_{Ti}	0.0171	0.0175	0.0170[6]
Δz_{O1}	-0.0189	-0.0186	-0.0110[6]
Δy_{O2}	0.0086	-	0.0061[6]
Δz_{O2}	-0.0185	-	-0.0157[6]
B (GPa)	115	109	-
E_g (eV)	4.6	4.7	-
ΔE^c (mHa)	-1.56	-2.06	-
Rhombohedral (R3m)			
a (Å)	4.010	4.029	4.004[6]
α (deg)	89.800	89.727	89.839[6]
V (Å^3)	64.47	-	64.17[6]
Δx_{Ti}	-0.0132	-0.0151	-0.0128[6]
Δx_O	0.0232	0.0129	0.0109[6]
Δz_O	0.0124	0.0242	0.0193[6]
B (GPa)	121	114	-
E_g (eV)	4.8	4.9	-
ΔE^c (mHa)	-1.62	-2.24	-

[a] Ambient pressure, high temperature from Ref. 13

[b] Room temperature, 1.6 GPa from Ref. 72

[c] Computed from the elastic constants of Ref. 41

Upon cooling, at 393 K, the paraelectric cubic structure undergoes a ferroelectric phase transition to a tetragonal phase, with space group P4mm, that contains four symmetry-irreducible atoms in the cell; with respect to the cubic lattice, Ti and O atoms are displaced along the z direction, as indicated in Table I. Below 278 K, symmetry is further reduced to orthorhombic (space group Amm2) with four symmetry-irreducible atoms in the cell; with respect to the tetragonal phase, the second O atom is displaced also along the y direction. Eventually, below 183 K, a rhombohedral ferroelectric phase with space group R3m, is found with three symmetry-irreducible atoms per cell: whereas Ba remains fixed at the origin of the cell, both Ti and O atoms are displaced along the three Cartesian axes, as shown in Table I.

Structural and electronic properties of the four phases of $BaTiO_3$ are given in Table II, as theoretically determined in this study at the PBE0 level and compared with existing experimental data and a previous theoretical investigation, at PBE0 level, by Evarestov and Bandura.[20] Lattice parameters a, b, c, volume V, bulk modulus B, electronic direct band-gap E_g and atomic positions, as defined in Table I, are reported. For the rhombohedral phase, the lattice angle α is also shown. For each ferroelectric phase, its energy difference ΔE_c with respect to the cubic phase is given.

As previously observed for other perovskites,[48,73] the PBE0 hybrid functional is providing a fairly reasonable description of the volume of the four systems under investigation, the largest deviation from experiment being the underestimation by 1.27 % in the cubic phase; a slight underestimation by 0.26 % is found for the tetragonal phase while slight overestimations by 0.22 % and 0.47 % are obtained for the orthorhombic and rhombohedral phases. In this respect, underestimations of the volume of the two high-temperature cubic and tetragonal phases can be easily understood in terms of the lack of any thermal lattice expansion in the calculations, which refer to 0 K. The computed bulk modulus B of the cubic phase, 194 GPa, compares with the experimental value at a pressure of 1.6 GPa, 195 GPa, thus indirectly confirming the underestimation of the volume. The theoretical bulk moduli of the three ferroelectric phases are much smaller than that of the cubic phase, as also partially confirmed by available experimental data for the tetragonal phase, 134-141 GPa, with respect to 162-195 GPa for the cubic phase. Our computed bulk moduli are obtained by fitting energy-volume data-points to the universal exponential Vinet's equation of state.[74]

Beside volume, also atomic displacements from their cubic sites to form the ferroelectric phases are relatively well described at this level of theory. Even if the absolute values of the direct band-gap of the cubic and tetragonal phases deviate from the experimental data by 0.8 eV, the 0.2 eV increase of the band-gap from the cubic to the tetragonal phase is perfectly reproduced. As a further internal check for consistency, the energy difference ΔE_c of the ferroelectric phases with respect to the cubic one

TABLE III: Computed vibration frequencies of the optical phonon modes for the four different phases of $BaTiO_3$ as compared with available experimental data. For the tetragonal, orthorhombic and rhombohedral phases, the measured frequencies are taken from Ref. 32, Ref. 34 and Ref. 35, respectively. The longitudinal-optical/transverse-optical (LO/TO) splitting has been computed. Theoretical values of the infrared (IR) intensities are also reported for TO modes. Phonon modes are labeled according to the irreducible representation (irrep) they belong to. Imaginary frequencies are labeled with i.

Cubic			Tetragonal				Orthorhombic				Rhombohedral			
Mode (irrep)	$\nu_{\rm calc}$ ($\rm cm^{-1}$)	$\mathcal{I}_{\rm calc}$ (km/mol)	Mode (irrep)	$\nu_{\rm calc}$ ($\rm cm^{-1}$)	$\nu_{\rm exp}$ ($\rm cm^{-1}$)	$\mathcal{I}_{\rm calc}$ (km/mol)	Mode (irrep)	$\nu_{\rm calc}$ ($\rm cm^{-1}$)	$\nu_{\rm exp}$ ($\rm cm^{-1}$)	$\mathcal{I}_{\rm calc}$ (km/mol)	Mode (irrep)	$\nu_{\rm calc}$ ($\rm cm^{-1}$)	$\nu_{\rm exp}$ ($\rm cm^{-1}$)	$\mathcal{I}_{\rm calc}$ (km/mol)
TO			TO				TO				TO			
T_{1u}	$i230$	-	E	$i128$	soft	-	B_2	$i71$		-	A_1	176	173	186
T_{1u}	193	453	A	168	175	237	B_1	174		313	E	180		575
T_{2u}	317	not active	E	182	181	247	A_1	178		not active	E	245		4681
T_{1u}	489	60	B	303	silent	not active	B_2	180	193	115	A_2	302	silent	not active
LO			E	316	306	30	B_1	285	270	1872	E	318		not active
T_{1u}	180		A	373	275	1308	B_1	302		301	A_1	320	242	1539
T_{1u}	486		E	487	487	105	A_2	316	320	not active	E	491		347
T_{1u}	694		A	566	516	648	A_1	318		not active	A_1	557	522	325
			LO				A_1	345		16	LO			
			E	176	180		B_2	487	490	59	E	188		
			A	199	191		B_1	496		270	A_1	193	187	
			E	315	305		A_1	562	532	198	E	318	310	
			E	479	468		LO				E	473		
			A	492	471		B_2	176			A_1	503	485	
			E	701	717		A_1	178			A_1	729	714	
			A	775	725		B_1	190			E	739		
							B_1	300						
							A_1	318	320					
							A_1	349						
							B_1	472						
							B_2	477						
							A_1	594						
							B_2	704						
							B_2	752	720					

is found to regularly increase, in absolute value, while going down the phase transition series from tetragonal to rhombohedral, according to their relative stability at 0 K.

According to the displacive model, ferroelectric phase transitions in $BaTiO_3$ are driven by soft phonon modes.[8] The structural features of the ferroelectric phases are then very closely connected to their vibrational properties. In Table III, we report computed phonon frequencies of both transverse-optical (TO) and longitudinal-optical (LO) modes, as compared with available experimental data. To the best of our knowledge, no experimental phonon frequency data have been reported for the cubic phase while a number of theoretical simulations have been performed.[20,21,25,26,28] A quite complete experimental characterization is reported for the tetragonal phase spectrum[32] while few phonon frequency values are reported for the orthorhombic and rhombohedral phases.[34,35] All phonon modes in the table are labeled according to the symmetry irreducible representation (irrep) they belong to. Infrared (IR) intensities $\mathcal{I}_{\rm calc}$ for the TO modes are also reported, as computed for each mode p by means of the mass-weighted effective mode Born charge vector $\mathbf{Z}_p$,[75,76] evaluated through a Berry phase approach:[77,78]

$$\mathcal{I}_p = \frac{\pi}{3}\frac{N_A}{c^2} d_p \left|\mathbf{Z}_p\right|^2 \quad \text{with} \quad \left|\mathbf{Z}_p\right|^2 = \left|\frac{\partial \boldsymbol{\mu}}{\partial Q_p}\right|^2 , \qquad (6)$$

where N_A is Avogadro's number, c the speed of light, d_p the degeneracy of the p-th mode, $\boldsymbol{\mu}$ the cell dipole moment and Q_p the normal mode displacement coordinate. More details on the calculation of the infrared intensities in the CRYSTAL program can be found in Ref. 79.

Since our simulations are performed at 0 K, soft phonon modes driving the transitions from the cubic to

the tetragonal and orthorhombic phases are projected down to absolute zero and, thus, show imaginary frequencies. As expected, the low-temperature rhombohedral phase is characterized by phonon frequencies which are all positive that implies its stability at 0 K. In particular, for the cubic phase, we find an imaginary frequency of $i230$ cm^{-1} that is comparable to $i240$ cm^{-1} and $i257$ cm^{-1} obtained by Evarestov and Bandura in their recent *ab initio* periodic study at PBE and PBE0 level of theory, respectively.[20] For the tetragonal phase, calculated optical phonon frequencies are in good agreement with the rich set of experimental values measured by Nakamura.[32] The only significant deviation refers to a TO phonon mode belonging to the totally-symmetric A irrep, for which the calculated value is 373 cm^{-1} and the measured one 275 cm^{-1}.

For the orthorhombic and rhombohedral ferroelectric phases, few experimental phonon frequencies are reported, in good agreement with our simulated values, with the exception of a single TO mode of A_1 symmetry of the rhombohedral phase where the computed value of 320 cm^{-1} largely overestimates the experimental value of 242 cm^{-1}. Given the overall good agreement with the experimental data, such few deviations are likely to be due to specific problems in extracting the correct vibration frequencies from incomplete experimental spectra.

B. The Rhombohedral Phase

In this section, dielectric, elastic, piezoelectric and photoelastic properties of the low-temperature rhombohedral phase of $BaTiO_3$ are discussed and the effect on these properties of the adopted one-electron Hamiltonian is investigated.

1. *Dielectric Tensor*

Given the relatively high symmetry of the system, there are only two independent components in the optical (*i.e.* purely electronic) dielectric tensor: ϵ_{11} and ϵ_{33}. They were computed as a function of the electric field wavelength λ with four different one-electron Hamiltonians: HF, PBE0, LDA and PBE (Figure 1). From previous applications of the CPHF/KS method, we know that the generalized-gradient approximation to the DFT, such as the PBE functional, usually provides the best agreement with experimental dielectric tensors, even better than hybrid schemes when the crystal structure, including cell parameters, is fully relaxed.[62,80]

All the Hamiltonians describe $\epsilon_{11} > \epsilon_{33}$. The HF method gives very small values of dielectric constants, relatively close to each other and almost independent on the electric field wavelength λ. Pure DFT functionals, PBE and LDA, predict much larger values (LDA more so than PBE), with a larger separation between them and with a strong dependence on λ. As expected, the hybrid

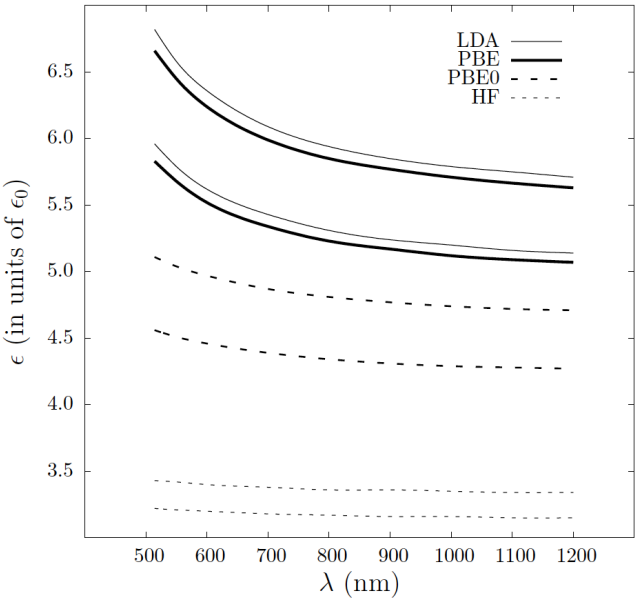

FIG. 1: For each considered Hamiltonian, the two dielectric constants ϵ_{11} and ϵ_{33} (in units of ϵ_0) are reported as a function of the electric field wavelength λ, for the rhombohedral phase; $\epsilon_{11} > \epsilon_{33}$ in all cases.

PBE0 functional provides an intermediate description of the dielectric constants, in all respects.

As clearly seen from pure DFT and hybrid data, which are known to accurately describe dielectric properties of solids, the explicit account of the dependence of computed dielectric response properties on the electric field wavelength λ is found to be mandatory before any comparison with future experiments which, as usual, will be performed at finite (and relatively small) values of λ (between 500 nm and 600 nm).

Two previous theoretical studies, one by Wu *et al.*[31] in 2005 and one by Evarestov and Bandura[20] in 2012, discussed their results of the dielectric constants of the rhombohedral phase of $BaTiO_3$ comparing with what they assumed to be the corresponding experimental counterpart, that is, data from Ref. 81 (2001). As a matter of fact, the values reported in Ref. 81 are in turn taken from a much earlier study by Wemple *et al.*[71] (1968) which, however, refers to the room-temperature tetragonal phase of $BaTiO_3$ (see Figure 4 therein and the related discussion). In that work, the authors also explicitly measured the λ-dependence of the dielectric constants, in the 400 nm - 700 nm range, which was found to be rather strong.

2. *Elastic and Photoelastic Properties*

Predicted elastic and photoelastic properties of low-temperature $BaTiO_3$, with four different Hamiltonians, are given in Table IV. In particular, elasto-optic constants here refer to the $\lambda \to \infty$ limit; see below for

TABLE IV: Elastic and photoelastic constants of the rhombohedral phase of $BaTiO_3$ as computed with four different one-electron Hamiltonians. The density ρ, along with a number of polycrystalline aggregate elastic properties, such as bulk modulus $\overline{B}$, shear modulus $\overline{G}$, Young's modulus E, Poisson's ratio σ and transverse, $\overline{v}_s$, and longitudinal, $\overline{v}_p$, seismic wave velocities, are also reported. Electronic "clamped-ion" and total "nuclear-relaxed" values are reported for each quantity.

	Elastic Constants (GPa)							Photoelastic Constants							ρ	$\overline{B}$	$\overline{G}$	E	σ	$\overline{v}_s$	$\overline{v}_p$
	C_{11}	C_{12}	C_{13}	C_{14}	C_{33}	C_{44}	C_{66}	p_{11}	p_{12}	p_{13}	p_{14}	p_{33}	p_{44}	p_{66}	(g/cm^3)	(GPa)	(GPa)	(GPa)		(km/s)	(km/s)
HF																					
Relaxed	290	66	1	76	282	45	112	0.074	0.241	0.249	-0.097	0.467	0.125	-0.083	5.92	110	41	109	0.33	2.6	5.3
Clamped	399	116	91	28	395	116	141	0.036	0.096	0.143	-0.046	0.043	0.001	-0.030	5.92	199	131	322	0.23	4.7	7.9
LDA																					
Relaxed	327	96	64	34	319	83	116	0.228	0.169	0.314	-0.169	0.510	0.207	0.030	6.31	158	99	245	0.24	4.0	6.8
Clamped	381	119	109	9	377	122	131	-0.026	-0.010	0.032	-0.041	-0.034	0.022	-0.008	6.31	202	128	317	0.24	4.5	7.7
PBE																					
Relaxed	250	70	31	43	226	39	90	0.217	0.185	0.341	-0.166	0.558	0.261	0.016	5.85	109	52	134	0.29	3.0	5.5
Clamped	323	101	85	12	299	95	111	-0.053	0.002	0.069	-0.035	0.005	0.005	-0.027	5.85	165	105	259	0.23	4.2	7.2
PBE0																					
Relaxed	282	73	31	47	258	44	104	0.161	0.193	0.299	-0.140	0.500	0.213	-0.016	6.02	121	61	156	0.28	3.2	5.8
Clamped	365	113	94	14	340	108	126	-0.032	0.032	0.098	-0.041	0.018	0.002	-0.032	6.02	185	118	293	0.24	4.8	7.5

an explicit account of electric field wavelength dependence. Unfortunately, no experimental data are currently available to compare with. From previous studies, we expect the hybrid PBE0 scheme to give the best description of elastic properties and the PBE functional the best description of photoelastic properties.[47,49] Electronic "clamped-ion" and total "nuclear-relaxed" values are reported; their difference corresponds to the nuclear relaxation term, which is found to be dramatic. Even with a balanced Hamiltonian, such as PBE, it can be as large as twice the electronic contribution (see, for instance, C_{13} and C_{14}).

Elastic properties of isotropic polycrystalline aggregates can be computed from the elastic and compliance constants defined in Section II B via the so-called Voigt-Reuss-Hill averaging scheme.[82] For a rhombohedral crystal, the adiabatic bulk modulus is defined as the average $\overline{B} = \frac{1}{2}[B_V + B_R]$ between Voigt upper and Reuss lower bounds:

$$\begin{aligned} B_V &= \frac{1}{9}(2C_{11} + C_{33} + 2C_{12} + 4C_{13}) \\ B_R &= (2S_{11} + S_{33} + 2S_{12} + 4S_{13})^{-1} \, . \end{aligned}$$

The shear modulus $\overline{G} = \frac{1}{2}[G_V + G_R]$ is expressed as the average between Voigt upper G_V and Reuss lower G_R bounds:

$$\begin{aligned} G_V &= \frac{1}{15}(2C_{11} + C_{33} - C_{12} - 2C_{13} + 6C_{44} + 3C_{66}) \\ G_R &= 15(8S_{11} + 4S_{33} - 4S_{12} - 8S_{13} + 6S_{44} + 3S_{66}) \, . \end{aligned}$$

From the average bulk and shear moduli defined above, Young's modulus E and Poisson's ratio σ are defined as follows:

$$E = \frac{9\overline{B}\,\overline{G}}{3\overline{B} + \overline{G}} \quad \text{and} \quad \sigma = \frac{3\overline{B} - 2\overline{G}}{2(3\overline{B} + \overline{G})} \, . \tag{7}$$

According to the elastic continuum theory, the three acoustic wave velocities of a crystal, along any general direction, are related to the elastic constants by Christoffel's equation.[83,84] Within the Voigt-Reuss-Hill averaging scheme, the average values of transverse (shear), $\overline{v}_s$, and longitudinal, $\overline{v}_p$, seismic wave velocities, for an isotropic polycrystalline aggregate, can be computed from the elastic properties defined above and the density ρ of the crystal as:[85]

$$\overline{v}_s = \sqrt{\frac{\overline{G}}{\rho}} \quad \text{and} \quad \overline{v}_p = \sqrt{\frac{\overline{B} + \frac{4}{3}\overline{G}}{\rho}} \, . \tag{8}$$

All the elastic properties introduced above have been computed with different Hamiltonians for the rhombohedral low-temperature phase of $BaTiO_3$ and reported in Table IV. The relevance of the nuclear relaxation effect, which systematically reduces the rigidity of the system, can be clearly seen from all these average properties.

As stated above, the elasto-optic constants reported in Table IV, refer to the $\lambda \to \infty$ limit. Since Brillouin scattering experiments are usually performed at finite electric field wavelengths (500 nm $< \lambda <$ 600 nm), in order to facilitate the comparison with future experimental measurements, we have computed the explicit dependence

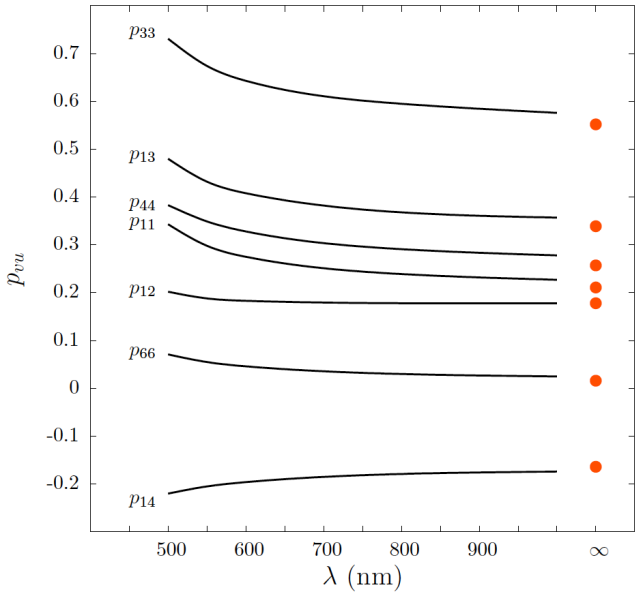

FIG. 2: (color online) Elasto-optic constants p_{vu} of the rhombohedral phase of $BaTiO_3$ as computed at PBE level, as a function of the electric field wavelength λ. Computed values at the $\lambda \to \infty$ limit are also reported as red circles.

of all these constants on λ at the PBE level: a wide range, from 500 nm to 1000 nm, is considered. Results are shown in Figure 2, along with simulated values at $\lambda \to \infty$. None of the elasto-optic constants changes sign as a function of λ. All six symmetry-independent positive components decrease with λ while the only negative one, p_{14}, increases with λ. Three constants, p_{12}, p_{66} and p_{14}, show a relatively small dependence on the field wavelength, whereas the remaining four more strongly depend on λ, particularly in the region between 500 nm and 600 nm.

3. *Piezoelectricity*

In recent years, the interest in the piezoelectric response of simple perovskites at very low temperature has been raised by the discovery, by Grupp and Goldman in 1997, of a giant piezoelectric effect of strontium titanate $SrTiO_3$ down to 1.6 K where piezoelectricity is usually severely reduced.[48,86] Such findings opened the way to applications of these materials at cryogenic temperatures as actuators for adaptive optics and low-temperature capacitors.

We report a complete characterization of the direct **e** and converse **d** third-order piezoelectric tensors of rhombohedral $BaTiO_3$, as introduced in Section II B. Piezoelectric constants are reported in Table V, as computed with four one-electron Hamiltonians. For this property, as for elastic constants, hybrid functionals, as PBE0, usually provide a rather good description. Total values are given along with purely electronic "clamped-ion" contributions. Nuclear relaxation effect plays here a fundamental role: three direct, symmetry-independent, piezoelectric constants out of four change their sign when including such an effect (e_{15}, e_{21} and e_{31}). In particular, the pure electronic contribution to e_{31} is predicted to be very small, 0.06 C/m^2. All these features agree with the outcomes of a previous LDA theoretical investigation, performed at the experimental volume.[31]

TABLE V: Direct and converse piezoelectric constants of the rhombohedral phase of $BaTiO_3$, as computed with four different Hamiltonians. Electronic and total nuclear relaxed values are given.

	Direct (C/m^2)				Converse (pm/V)			
	e_{15}	e_{21}	e_{31}	e_{33}	d_{15}	d_{21}	d_{31}	d_{33}
HF								
Relaxed	-7.52	3.24	-3.30	-4.41	1562[†]	-511[†]	-9.2	-15.6
Clamped	0.14	-0.19	0.06	-0.14	1.6	-0.8	0.2	-0.4
LDA								
Relaxed	-5.81	3.75	-4.77	-6.46	-95.0	30.3	-8.7	-16.8
Clamped	0.13	-0.15	0.04	-0.12	1.1	-0.6	0.2	-0.4
PBE								
Relaxed	-4.31	1.93	-2.11	-3.52	-290	80.6	-5.2	-14.1
Clamped	0.20	-0.28	0.05	-0.23	2.5	-1.4	0.3	-0.9
PBE0								
Relaxed	-4.67	1.99	-2.17	-3.45	-271	73.9	-5.0	-12.2
Clamped	0.21	-0.28	0.06	-0.22	2.3	-1.2	0.3	-0.8

[†] These unusual large values are due to very large elements of the HF compliance tensor $\mathbb{S} = \mathbb{C}^{-1}$ in this case.

Converse piezoelectricity depends on both the direct piezoelectric tensor and the elastic tensor (or its inverse, the compliance tensor). The hybrid PBE0 approach with full geometry optimization is found to provide results that are in good agreement with those of a previous LDA simulation, constrained at the experimental volume, where $d_{15} = -243.2$, $d_{21} = 70.1$, $d_{31} = -6.8$, $d_{33} = -14.7$.[31]

IV. CONCLUSIONS

Accurate *ab initio* simulations have been applied to the theoretical characterization of several tensorial properties of the low-temperature rhombohedral phase of barium titanate, $BaTiO_3$. Dielectric, elastic, piezoelectric and photoelastic tensors have been computed with four different one-electron Hamiltonians (including Hartree-Fock, here reported as a benchmark), representatives of four different levels of approximation. The explicit treatment of the dependence of dielectric and photoelastic constants on the electric field frequency provides with results that can be more directly compared with future experimental ones.

The adopted computational approach has been dis-

cussed by comparing computed with experimental structural and vibrational properties of four phases of $BaTiO_3$: cubic $Pm\overline{3}m$, tetragonal P4mm, orthorhombic Amm2 and rhombohedral R3m. The agreement with available experimental data and previous theoretical investigations is remarkable. In general, we expect predictions by the PBE0 hybrid functional to be the most reliable as regards elastic and piezoelectric properties of the rhombohedral phase whereas those by PBE to describe accurately dielectric and photoelastic properties.

In the analysis of available experimental data, we could realize that some experimental measurements of the dielectric constants of $BaTiO_3$ were wrongly assigned, by some authors of theoretical investigations, to the rhombohedral phase, and not to the correct phase, that is the tetragonal one, in past years.

Acknowledgments

Gustavo Sophia is kindly acknowledged for his support in the basis set optimization with the LoptCG script. The CINECA Award N. HP10BLSOR4-2012 is acknowledged for the availability of high performance computing resources and support. Improvements in the massive-parallel version of CRYSTAL09 were made possible thanks to the PRACE proposal no. 2011050810.

* Electronic address: agnesnora.mahmoud@unito.it

[1] M. E. Lines and A. M. Glass, *Principles and Applications of Ferroelectrics and Related Materials* (Oxford University Press, Oxford, 1977).
[2] J. F. Scott, *Ferroelectric Memories* (Springer-Verlag, Berlin, 2000).
[3] R. Waser, *Nanoelectronics and Information Technology* (Wiley-VCH, Weinheim, 2003).
[4] J. F. Scott, J. Phys.: Condens. Matter **18**, R361 (2006).
[5] W. Wul and I. M. Goldman, C. R. Acad. Sci. Russ. **46**, 139 (1945).
[6] G. H. Kwei, A. C. Lawson, and S. J. L. Billinge, J. Phys. Chem. **97**, 2368 (1993).
[7] P. Goudochnikov and A. J. Bell, J. Phys.: Condens. Matter **19**, 176201 (2007).
[8] W. Cochran, Adv. Phys. **9**, 387 (1960).
[9] I. B. Bersuker, Phys. Lett. **20**, 1966 (589-590).
[10] R. Comes, M. Lambert, and A. Guinier, Solid State Commun. **6**, 715 (1968).
[11] R. Comes, M. Lambert, and A. Guinier, Acta Crystallogr. Sec. A **26**, 244 (1970).
[12] J. W. Edwards, R. Speiser, and H. L. Johnston, J. Am. Chem. Soc. **73**, 2934 (1951).
[13] M. Adachi, Y. Akishige, T. Asahi, K. Deguchi, K. Gesi, K. Hasebe, T. Hikita, T. Ikeda, and Y. Iwata, *Ferroelectrics and Related Substances* (Springer-Verlag, 1981), vol. 16, chap. Oxides.
[14] B. C. Frazer, H. R. Danner, and R. Pepinsky, Phys. Rev. Lett. **100**, 745 (1955).
[15] H. T. Evans, Acta Crystallogr. Sec. A **14**, 1019 (1961).
[16] J. Harada, T. Pedersen, and Z. Barnea, Acta Crystallogr. Sec. A **26**, 336 (1970).
[17] G. Shirane, H. Danner, and R. Pepinsky, Phys. Rev. **105**, 856 (1957).
[18] A. W. Hewat, Ferroelectrics **6**, 215 (1973).
[19] W. Schildkamp and K. Fischer, Z. Kristallogr. **155**, 17 (1981).
[20] R. A. Evarestov and A. Bandura, J. Comp. Chem. **33**, 1123 (2012).
[21] R. A. Evarestov, Phys. Rev. B **83**, 014105 (2011).
[22] A. V. Bandura and R. A. Evarestov, J. Comput. Chem. **33**, 1554 (2012).
[23] Y.-S. Seo and J. S. Ahn, J. Korean Phys. Soc. **62**, 1629 (2013).
[24] A. I. Lebedev, Phys. Solid State **51**, 341 (2009).
[25] P. Ghosez, X. Gonze, and J.-P. Michenaud, Ferroelectrics **206**, 205 (1998).
[26] Q. Zhang, T. Cagin, and W. A. Goddard, Proc. Nat. Acad. Sci. **103**, 14695 (2006).
[27] R. D. King-Smith and D. Vanderbilt, Phys. Rev. B **49**, 5828 (1994).
[28] W. Zhong, R. D. King-Smith, and D. Vanderbilt, Phys. Rev. Lett. **72**, 3618 (1994).
[29] W. Zhong, D. Vanderbilt, and K. M. Rabe, Phys. Rev. B **52**, 6301 (1995).
[30] J. Íñiguez and D. Vanderbilt, Phys. Rev. Lett. **89**, 115503 (2002).
[31] X. Wu, D. Vanderbilt, and D. R. Hamann, Phys. Rev. B **72**, 035105 (2005).
[32] T. Nakamura, Ferroelectrics **137**, 65 (1992).
[33] U. D. Venkateswaran, V. M. Naik, and R. Naik, Phys. Rev. B **58**, 14256 (1998).
[34] K. Laabidi and M. D. Fontana, Solid State Commun. **76**, 765 (1990).
[35] D. A. Tenne, X. X. Xi, Y. L. Li, L. Q. Chen, A. Soukiassian, M. H. Zhu, A. R. James, J. Lettieri, D. G. Schlom, W. Tian, and X. Q. Pan, Phys. Rev. B **69**, 174101 (2004).
[36] S. Sanna, C. Thierfelder, S. Wippermann, T. P. Sinha, and W. G. Schmidt, Phys. Rev. B **83**, 054112 (2011).
[37] M. Uludogan, D. P. Guarin, Z. E. Gomez, T. Cagin, and W. A. G. III, Comput. Mod. Eng. Sci. **24**, 215 (2008).
[38] P. Hermet, M. Veithen, and P. Ghosez, J. Phys.: Condens. Matter **21**, 215901 (2009).
[39] N. Choudhury, E. J. Walter, A. I. Kolesnikov, and C.-K. Loong, Phys. Rev. B **77**, 134111 (2008).
[40] D. Berlincourt and H. Jaffe, Phys. Rev. **111**, 143 (1958).
[41] A. Schaefer, H. Schmitt, and A. Dorr, Ferroelectrics **69**, 253 (1986).
[42] A. Khalal, D. Khatib, and B. Jannot, Phys. B **271**, 343 (1999).
[43] M. Zgonik, P. Bernasconi, M. Duelli, R. Schlesser, P. Günter, M. H. G. D. Rytz, Y. Zhu, and X. Wu, Phys. Rev. B **50**, 5941 (1994).
[44] A. V. Turik, Soviet Physics-Solid State **12**, 688 (1970).
[45] M. G. Cohen, M. DiDomenico, and S. H. Wemple, Phys. Rev. B **1**, 4334 (1970).
[46] J. J. Wang, F. Y. Meng, X. Q. Ma, M. X. Xu, and L. Q. Chen, J. Appl. Phys. **108**, 034107 (2010).

[47] A. Erba, A. Mahmoud, R. Orlando, and R. Dovesi, Phys. Chem. Minerals (2013), doi: 10.1007/s00269-013-0630-4.
[48] A. Erba, K. E. El-Kelany, M. Ferrero, I. Baraille, and M. Rérat, Phys. Rev. B **88**, 035102 (2013).
[49] A. Erba and R. Dovesi, Phys. Rev. B **88**, 045121 (2013).
[50] A. Erba, M. Ferrabone, J. Baima, R. Orlando, M. Rérat, and R. Dovesi, J. Chem. Phys. **138**, 054906 (2013).
[51] J. P. Perdew, K. Burke, and M. Ernzerhof, Phys. Rev. Lett. **77**, 3865 (1996).
[52] C. Adamo and V. Barone, J. Chem. Phys. **110**, 6158 (1999).
[53] R. Dovesi, V. R. Saunders, C. Roetti, R. Orlando, C. M. Zicovich-Wilson, F. Pascale, K. Doll, N. M. Harrison, B. Civalleri, I. J. Bush, et al., *CRYSTAL09 User's Manual*, Università di Torino, Torino (2010), http://www.crystal.unito.it.
[54] R. Dovesi, R. Orlando, B. Civalleri, C. Roetti, V. R. Saunders, and C. M. Zicovich-Wilson, Z. Kristallogr. **220**, 571 (2005).
[55] C. Zicovich-Wilson, *Loptcg shell procedure for numerical gradient optimization* (1998).
[56] P. J. Hay and W. R. Wadt, J. Chem. Phys. **82**, 299 (1985).
[57] P. J. Hay and W. R. Wadt, J. Chem. Phys. **82**, 270 (1985).
[58] P. J. Hay and W. R. Wadt, J. Chem. Phys. **82**, 284 (1985).
[59] The basis set used in this work can be found in the CRYSTAL website following the link: http://www.crystal.unito.it/Basis_Sets/Ptable.html (2013).
[60] G. J. B. Hurst, M. Dupuis, and E. Clementi, J. Chem. Phys. **89**, 385 (1988).
[61] B. Kirtman, F. L. Gu, and D. M. Bishop, J. Chem. Phys. **113**, 1294 (2000).
[62] M. Ferrero, M. Rérat, R. Orlando, and R. Dovesi, J. Comp. Chem. **29**, 1450 (2008).
[63] C. Carteret, M. De La Pierre, M. Dossot, F. Pascale, A. Erba, and R. Dovesi, J. Chem. Phys. **138**, 014201 (2013).
[64] V. Lacivita, A. Erba, Y. Noël, R. Orlando, P. D'Arco, and R. Dovesi, J. Chem. Phys. **138**, 214706 (2013).
[65] J. Baima, A. Erba, R. Orlando, M. Rérat, and R. Dovesi, J. Phys. Chem. C **117**, 12864 (2013).
[66] J. F. Nye, *Physical properties of crystals* (Oxford University Press, Oxford, 1957).
[67] W. F. Perger, J. Criswell, B. Civalleri, and R. Dovesi, Comput. Phys. Commun. **180**, 1753 (2009).
[68] Y. Noel, C. M. Zicovich-Wilson, B. Civalleri, P. D'Arco, and R. Dovesi, Phys. Rev. B **65**, 014111 (2001).
[69] G. Saghi-Szabo, R. E. Cohen, and H. Krakauer, Phys. Rev. Lett. **80**, 4321 (1998).
[70] A. Dal Corso, M. Posternak, R. Resta, and A. Baldereschi, Phys. Rev. B **50**, 10715 (1994).
[71] S. Wemple, M. D. Jr., and I. Camlibel, J. Phys. Chem. Solids **29**, 1797 (1968).
[72] G. J. Fischer, Z. Wang, and S. Karato, Phys. Chem. Min. **20**, 97 (1993).
[73] G. Sophia, P. Baranek, C. Sarazzin, M. Rérat, and R. Dovesi, Phase Transition pp. 1–16 (2013).
[74] P. Vinet, J. Ferrante, J. H. Rose, and J. R. Smith, J. Geophys. Res.: Solid Earth **92**, 9319 (1987).
[75] G. M. Barrow, *Introduction to molecular spectroscopy* (McGraw-Hill, New York, 1962).
[76] B. A. Hess, L. J. Schaad, P. Carsky, and R. Zahradnik, Chem. Rev. **86**, 709 (1986).
[77] P. Baranek, C. M. Zicovich-Wilson, C. Roetti, R. Orlando, and R. Dovesi, Phys. Rev. B **64**, 125102 (2001).
[78] Y. Noël, C. M. Zicovich-Wilson, B. Civalleri, P. D'Arco, and R. Dovesi, Phys. Rev. B **65**, 014111 (2002).
[79] C. M. Zicovich-Wilson, F. J. Torres, F. Pascale, L. Valenzano, R. Orlando, and R. Dovesi, J. Comp. Chem. **29**, 2268 (2008).
[80] R. Orlando, V. Lacivita, R. Bast, and K. Ruud, J. Chem. Phys. **132**, 244106 (2010).
[81] B. Wang and C. Sun, Appl. Opt. **40**, 672 (2001).
[82] R. Hill, J. Mech. Phys. Solids **11**, 357 (1963).
[83] M. J. P. Musgrave, *Crystal Acoustics* (Holden-Day, San Francisco, California, 1970).
[84] B. A. Auld, *Acoustic Fields and Waves in Solids* (Krieger Publishing Company, Malabar, Florida, 1973).
[85] G. Ottonello, B. Civalleri, J. Ganguly, W. F. Perger, D. Belmonte, and M. Vetuschi Zuccolini, Am. Mineral. **95**, 563 (2010).
[86] D. E. Grupp and A. M. Goldman, Science **276**, 392 (1997).